

- Tubes [S. B. Shirey and R. J. Walker, *Anal. Chem.* **67**, 2136 (1995)] for ~48 hours at 230°C. After dissolution, the PGEs were isolated from one another and the bulk-rock matrix by anion-exchange chromatography [M. Rehkämper and A. N. Halliday, *Talanta* **44**, 663 (1997)]. The pure PGE fractions were then analyzed with a Plasma 54 multiple-collector inductively coupled plasma mass spectrometer [A. N. Halliday *et al.*, *Int. J. Mass Spectrom. Ion Processes* **146/147**, 21 (1995)]. Multiple analysis of Iceland basalt sample BTHO and Alexo komatiite sample KAL-1 demonstrate that our techniques achieve external reproducibilities of ~1.5 to 9% for the PGEs in the concentration range from parts per billion to parts per trillion. Duplicate analysis of two peridotite samples (OMX-8 and C235A) indicate a somewhat lower reproducibility ($\leq 15\%$), probably owing to the heterogeneity of the coarse-grained rocks. The PGE ratios of the duplicates, however, were identical to within 1 to 8%. Blanks for the Cameroon Line samples, digested with conventional Carius Tubes, were < 10 pg/g for Ru, Pd, and Ir and 100 to 200 pg/g for Pt. Northern Tanzanian xenoliths were digested with the use of a modified Carius Tube design, and this technique achieves blanks of < 15 pg/g for all analyzed PGEs [M. Rehkämper, A. N. Halliday, R. F. Wentz, *Fres. J. Anal. Chem.*, in press].
10. D.-C. Lee *et al.*, *J. Petrol.* **37**, 415 (1996).
 11. L. Cahen *et al.*, *The Geochronology and Evolution of Africa* (Clarendon, Oxford, UK, 1984); S. F. Toteu, A. Michard, J. M. Bertrand, G. Rocci, *Precambrian Res.* **37**, 71 (1987).
 12. J. B. Dawson, D. G. Powell, A. M. Reid, *J. Petrol.* **11**, 519 (1970); R. Hutchison and J. B. Dawson, *Earth Planet. Sci. Lett.* **9**, 87 (1970); W. I. Ridley and J. B. Dawson, in *Physics and Chemistry of the Earth*, L. H. Ahrens, J. B. Dawson, A. R. Duncan, A. J. Erlank, Eds. (Pergamon, New York, 1975), pp. 559–569.
 13. R. L. Rudnick, W. F. McDonough, A. Orpin, in *Proceedings of the Fifth International Kimberlite Conference*, Araxá, Brazil, 18 June to 4 July 1991, H. O. A. Meyer and O. Leonardos, Eds. (Companhia de Pesquisa de Recursos Minerais, Rio de Janeiro, Brazil, 1991), vol. 1, pp. 336–353.
 14. R. L. Rudnick, W. F. McDonough, B. W. Chappell, *Earth Planet. Sci. Lett.* **114**, 463 (1993).
 15. P. H. Nixon, in *Mantle Xenoliths*, P. H. Nixon, Ed. (Wiley, Chichester, UK, 1987), pp. 215–240.
 16. S. E. Kesson and A. E. Ringwood, *Chem. Geol.* **78**, 97 (1989).
 17. R. S. Cohen, R. K. O'Nions, J. B. Dawson, *Earth Planet. Sci. Lett.* **68**, 209 (1984).
 18. J. B. Dawson, in *Mantle Metasomatism*, M. A. Menzies and C. J. Hawkesworth, Eds. (Academic Press, London, 1987), pp. 125–144.
 19. N. J. Page, J. S. Pallister, M. A. Brown, J. D. Smewing, J. Haffty, *Can. Mineral.* **20**, 537 (1982); N. J. Page and R. W. Talkington, *ibid.* **22**, 137 (1984); N. J. Page, T. Engin, D. A. Singer, J. Haffty, *Econ. Geol.* **79**, 177 (1984); A. Cocherie, T. Augé, G. Meyer, *Chem. Geol.* **77**, 27 (1989); B. McElduff and E. F. Stumpfl, *Mineral. Petrol.* **42**, 211 (1990); M. Leblanc, *Econ. Geol.* **90**, 2028 (1995); J. Vuollo *et al.*, *ibid.*, p. 445.
 20. H. J. B. Dick and T. Bullen, *Contrib. Mineral. Petrol.* **86**, 54 (1984).
 21. J. A. Pearce, S. J. Lippard, S. Roberts, in *Marginal Basin Geology*, B. P. Kokelaar and M. F. Howells, Eds. (Blackwell, Oxford, UK, 1984), pp. 77–94; D. Elthon, *Nature* **354**, 140 (1991).
 22. G. Agiorgitis and R. Wolf, *Chem. Geol.* **23**, 267 (1978); I. O. Oshin and J. H. Crockett, *Econ. Geol.* **77**, 1556 (1982); C. J. Copobianco, R. L. Hervig, M. J. Drake, *Chem. Geol.* **113**, 23 (1994).
 23. Spinel from fertile western Australian lherzolites, for example, are characterized by superchondritic Pd/Ir ratios (2), as are chromitites from stratiform chromite deposits [C. McLaren and J. P. R. De Villiers, *Econ. Geol.* **77**, 1348 (1982); S. J. Perry, *Chem. Geol.* **43**, 115 (1984)]. Furthermore, a large proportion of the PGE budget of fertile peridotite xenoliths appears to be contained in acid-leachable, intergranular sulfide phases, whereas spinel is only a minor host for the PGEs (2) [S. R. Hart and G. E. Ravizza, in *Earth Processes: Reading the Isotopic Code*, A. Basu and S. R. Hart, Eds. (American Geophysical Union, Washington, DC, 1996), pp. 123–134]. Although chromitites from ophiolite complexes are characterized by high PGE abundances, a number of detailed studies demonstrate that the PGEs are not incorporated into the lattice of the chromites but are concentrated in sulfide and alloy inclusions; the chromites themselves have no bearing on the fractionation of the PGEs [for example, H. W. Stockmann and P. F. Hlava, *Econ. Geol.* **79**, 491 (1984); R. W. Talkington, D. H. Watkinson, P. J. Whittaker, P. C. Jones, *Tschermaks Mineral. Petrogr. Mitt.* **32**, 285 (1984); R. J. Walker, E. Hanski, J. Vuollo, J. Liipo, *Earth Planet. Sci. Lett.* **141**, 161 (1996)].
 24. Three abyssal harzburgites from the MARK area (Mid-Atlantic Ridge, Kane Fracture Zone) with $< 1.0\%$ CaO are characterized by suprachondritic Pd/Ir ratios and Pt/Ru ratios that are only marginally subchondritic (M. Rehkämper *et al.*, in preparation). Two harzburgites from the Horomann peridotite (CaO $< 0.5\%$), generally considered to represent former suboceanic mantle lithosphere, have Pd/Ir ratios of 0.15 to 0.20 but higher-than-chondritic ratios of Pt/Ir and Pt/Ru [E. Takazawa, thesis, MIT (1996); M. Rehkämper *et al.*, in preparation]. These characteristics are remarkably similar to the results for harzburgite sample N12 from the Cameroon Line (this study). Six harzburgites and dunites from the Ronda and Beni Bousera massifs with 0.3 to 1% CaO display a wide range of Pd/Ir ratios (0.24 to 1.44) and Pt/Ru ratios (0.31 to 2.40) (6). These values are significantly larger, by at least a factor of 5, than the minimum ratios recorded for the northern Tanzanian xenoliths.
 25. I. Kushiro, *Am. J. Sci.* **267-A**, 269 (1969).
 26. Z. Johann, H. Dunlop, L. Le Bel, J. L. Robert, M. Volfiner, *Fortschr. Mineral.* **61**, 105 (1983); P. Schiano *et al.*, *Earth Planet. Sci. Lett.* **146**, 489 (1997).
 27. S. A. Wood, *Geochim. Cosmochim. Acta* **51**, 3041 (1987); M. E. Fleet and T.-W. Wu, *ibid.* **57**, 3519 (1993).
 28. R. R. Keays, E. H. Nickel, D. I. Groves, P. J. McGoldrick, *Econ. Geol.* **77**, 1535 (1982); C. G. Ballhaus and E. F. Stumpfl, *Contrib. Mineral. Petrol.* **94**, 193 (1986); A. D. Brandon, R. A. Creaser, S. B. Shirey, R. W. Carlson, *Science* **272**, 861 (1996).
 29. J. T. Wasson and G. W. Kallemeyn, *Philos. Trans. R. Soc. London Ser. A* **325**, 535 (1988).
 30. K. P. Jochum, *Geochim. Cosmochim. Acta* **60**, 3353 (1996).
 31. G. W. Kallemeyn and J. T. Wasson, *ibid.* **50**, 2153 (1986).
 32. W. F. McDonough and S.-s. Sun, *Chem. Geol.* **120**, 223 (1995).
 33. We thank M. Johnson, D.-C. Lee, J. Christensen, C. Hall, D. Teagle, and the other members of the RIGL team for help in keeping the P54 running smoothly and for many fruitful discussions; C. Paslick for field assistance; D. Bugocki and W. Yi for vital assistance during sample preparation; and S. Mukasa and J. Zipfel for helpful comments. Three anonymous referees provided very thorough and helpful reviews. This research was supported by NSF grants EAR 94-06248 and EAR 96-14457 and by DOE grant DE-FG02-94ER14412.

2 June 1997; accepted 20 October 1997

Transitions Between Blocked and Zonal Flows in a Rotating Annulus with Topography

Eric R. Weeks, Yudong Tian, J. S. Urbach,* Kayo Ide, Harry L. Swinney,† Michael Ghil

The mid-latitude atmosphere is dominated by westerly, nearly zonal flow. Occasionally, this flow is deflected poleward by blocking anticyclones that persist for 10 days or longer. Experiments in a rotating annulus used radial pumping to generate a zonal jet under the action of the Coriolis force. In the presence of two symmetric ridges at the bottom of the annulus, the resulting flows were nearly zonal at high forcing or blocked at low forcing. Intermittent switching between blocked and zonal patterns occurs because of the jet's interaction with the topography. These results shed further light on previous atmospheric observations and numerical simulations.

On short time scales (1 to 10 days), weather evolution is largely driven by three-dimensional, baroclinic instabilities of the prevailing westerlies (1) that convert the potential energy in the atmosphere's pole-to-equator temperature difference into the kinetic energy of storms (2). One to three times each Northern Hemisphere winter—and occasionally during other seasons—large high-pressure anticyclones form and persist for at least 10 days and sometimes longer than a

month (3–5). These anticyclones block the nearly zonal flow and deflect it poleward (Fig. 1B). The prediction of blocking events has become central to improving extended-range weather prediction (6, 7).

Low-frequency atmospheric variability on the time scale of 10 to 100 days, such as persistent blocking anomalies, is predominantly barotropic, that is, nearly two-dimensional (5, 8, 9). Analytic and numerical models have shown that blocked and zonal flow patterns can arise through the interaction of large-scale eastward zonal flow with idealized Northern Hemisphere topography (7, 8, 10–12), and recent numerical simulations using a general circulation model (13) support these results. Zonal and blocked flows appear as two stable equilibria (8, 10, 11) or two separate chaotic flow regimes (12, 14–16) in simple and intermediate models.

E. R. Weeks, J. S. Urbach, H. L. Swinney, Center for Nonlinear Dynamics and Department of Physics, University of Texas at Austin, Austin, TX 78712, USA.
Y. Tian, K. Ide, M. Ghil, Department of Atmospheric Sciences and Institute of Geophysics and Planetary Physics, University of California, Los Angeles, CA 90095, USA.

*Present address: Department of Physics, Georgetown University, Washington, DC 20057, USA.

†To whom correspondence should be addressed. E-mail: swinney@chaos.ph.utexas.edu

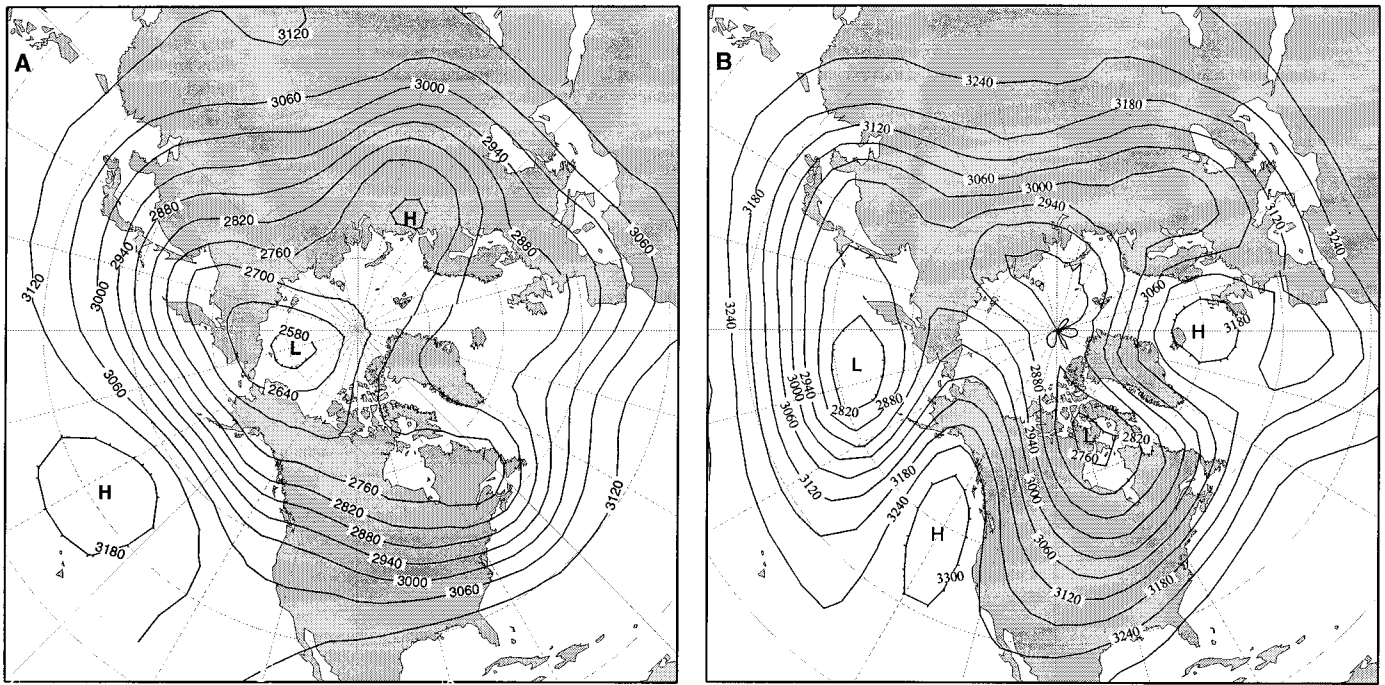


Fig. 1. Atmospheric pictures of (A) zonal and (B) blocked flow, showing contour plots of the height (m) of the 700-hPa (700 mbar) surface, with a contour interval of 60 m for both panels. The plots were obtained by averaging 10 days of twice-daily data for (A) 13 to 22 December 1978 and (B) 10 to 19 January 1963; the data are from the National Oceanic and Atmospheric

Administration's Climate Analysis Center. The nearly zonal flow of (A) includes quasi-stationary, small-amplitude waves (32). Blocked flow advects cold Arctic air southward over eastern North America or Europe, while decreasing precipitation in the continent's western part (26).

Laboratory experiments in rotating annuli with a radial temperature gradient have helped in the understanding of the mechanism of baroclinic instability and the atmosphere's general circulation (17). Introducing wavenumber 2 topography in such annuli produced new phenomena (18) but did not adequately explain the spatiotemporal features of the atmosphere's observed and modeled low-frequency variability (19).

To further understand the dynamics of zonal flow over topography, we carried out laboratory experiments on a barotropic rotating annulus (20, 21) with two mountain ridges. The flow was produced by mechanical pumping and suction rather than by differential heating of the side walls (17). With the rapid rotation and absence of buoyant driving forces, the flow in the annulus was essentially two-dimensional (21) and could be compared with barotropic model results. These experiments facilitate exploration of the flow's behavior over a wide parameter range: an hour at a rotation frequency of 2 Hz corresponds to 20 simulated years.

The annular tank's inner radius $r_1 = 10.8$ cm, its outer radius $r_2 = 4r_1$, and its height varied linearly from 17.1 cm at the inner to 20.3 cm at the outer radius. Flow was produced by pumping fluid in through a ring of 120 holes (0.26 cm in diameter) at $r_{\text{source}} = (3.25)r_1$ and out through a ring of holes at $r_{\text{sink}} = (1.75)r_1$. The annulus was filled with water (kinematic viscosity $\nu =$

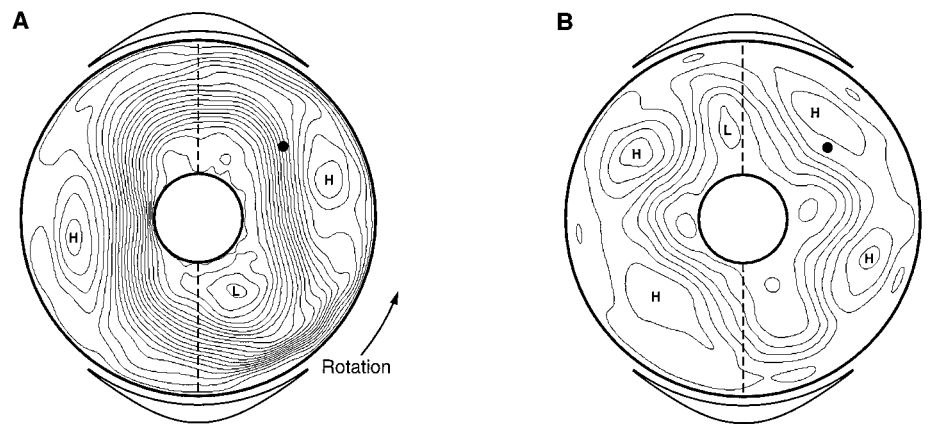


Fig. 2. Time-averaged stream function contours calculated from experimental data for (A) zonal and (B) blocked flow. The peaks of the ridges are indicated by dashed lines, and the profile of each ridge is shown by black curves outside the rim of the round panels. The contour interval is $15 \text{ cm}^2 \text{ s}^{-1}$ for both plots. The annulus rotates counterclockwise, and the flow is in the direction of rotation (eastward). The Rossby numbers Ro for the zonal and blocked flows are 0.33 ± 0.02 and 0.22 ± 0.02 , respectively (pump flux $F = 390$ and $260 \text{ cm}^3 \text{ s}^{-1}$, respectively); for both flows, the Ekman number $Ek = 4.8 \times 10^{-4}$ ($\Omega = 3\pi \text{ rad s}^{-1}$). A video camera was used to track neutrally buoyant particles of 1 mm diameter, and time-averaged stream functions were determined by averaging the particle trajectories in time (23) and fitting the results to basis functions. The highs and lows of the stream function are indicated by bold letters H and L, respectively. The black dots indicate the horizontal location of the hot-film probe.

$0.009 \text{ cm}^2 \text{ s}^{-1}$) up to a flat lid. When the tank rotated rapidly, the action of the Coriolis force on the radial flow resulted in a corotating (eastward) jet with a much higher velocity than the radial flow generated directly by the pumping (20, 21). The sloping bottom of the annulus models the

change in Coriolis force as a function of latitude for spherical planets [the β effect, which in the present case is given by $\beta = 2\Omega s/h$, where $s = 0.1$ is the slope, $h = 18.7$ cm is the mean height of the annulus, and Ω is the angular velocity of the annulus (21)]. Two radial aluminum ridges were

symmetrically placed on the bottom of the annulus, each having a Gaussian profile $h(r, \theta) = h(\theta) = h_0 \exp[-(\theta/\theta_0)^2]$ with $h_0 = 1.5$ cm and $\theta_0 = 21^\circ$. This profile extends over 72° ; at 72° the Gaussian profile is smoothly tapered to zero.

Our two control parameters were the pump flux rate F , which ranged from 0 to $400 \text{ cm}^3 \text{ s}^{-1}$, and Ω , which ranged from 2π to $6\pi \text{ rad s}^{-1}$ (1 to 3 Hz). These two control parameters determine the nondimensional Rossby (Ro) and Ekman (Ek) numbers. The Rossby number $Ro = U/2\Omega L$ is given in terms of L , the spacing between the forcing rings ($1.5r_1$), and the maximum velocity U that would result from a steady, axisymmetric flow in the absence of topography, $U = (F/2\pi) - (\Omega/\nu)^{1/2} r_{\text{sink}}^{-1}$ (21). The Ekman number is $Ek = (T_{\text{annulus}}/T_{\text{Ekman}})^2$, where $T_{\text{annulus}} = 2\pi/\Omega$ is the annulus rotation period and $T_{\text{Ekman}} = h/2(\nu\Omega)^{1/2}$ is the relaxation time for unforced disturbances (22); hence, $Ek = (4\pi/h)^2 (\nu/\Omega)$. In these experiments, $0.10 < Ro < 0.35$ and $0.4 \times 10^{-3} < Ek < 10^{-3}$.

In the absence of topography, the flow in this parameter range was characterized by eastward-propagating Rossby waves (21). With the topography in place, however, we observed two stationary wave patterns that had markedly different characteristics, as illustrated by the contour plots of typical time-averaged stream functions (Fig. 2) (23). At high Rossby numbers (that is, high pumping or low rotation), a nearly zonal flow (Fig. 2A), resembling the more frequently occurring atmospheric patterns (Fig. 1A), was observed: a strong corotating jet flowed smoothly around the annulus; it had a small-amplitude wave of zonal wavenumber 2 induced by the two mountains. At lower Rossby numbers, a blocked flow was observed (Fig. 2B); the jet was wavier, and its speed was much lower (see also Fig. 3, A and C). The azimuthal flux carried by the blocked jet was typically one-third that in the zonal jet, even for similar pumping rates and Ekman number (24). A strong wavenumber 4 component of the flow field arose; one anticyclone (counterrotating

vortex) formed upstream of each mountain, and the other formed downstream, like in a Rossby lee wave (25). In the atmosphere, though, unlike in our experiment, it is the upstream ridge (poleward curvature of the jet) that is more pronounced.

Blocking anticyclones appear in the atmosphere most often separately, in either the Pacific–North American or the North Atlantic–European sector, although double-blocking episodes (Fig. 1B) do occur (4, 5, 7, 26). The twofold symmetry of the apparatus presumably favors a double-blocking pattern. The drop in jet intensity, increase in wave amplitude, and upstream shift of the two stronger highs that we observed for blocked flow are in agreement with the simplified barotropic models (8, 10, 12, 27), which are supported by general circulation model results (13). Still, direct comparison of the experimental observations with the atmosphere is not possible, because the spectrum of Northern Hemisphere topography is dominated by wavenumbers 2 and 3, and thermal contrasts between continents and oceans also play an important role, as do baroclinic phenomena (10, 11, 14, 16).

The variability of the blocked flow in the experiments was much higher than that of the zonal flow. For zonal flow (Fig. 2A), the variations from the mean spatial pattern were small, and the instantaneous stream function resembled the time average. For blocked flow (Fig. 2B), the instantaneous patterns differed considerably from the time average over most of the parameter range investigated. The velocity time series for zonal flow, measured at a fixed point in the fluid, also showed that nearly periodic variations (with a period of 17 annulus rotations) were superimposed on a noisy background (Fig. 3, A and B) (16). The blocked flow had a broad-band spectrum, with spectral power P decreasing with frequency f (Fig. 3D). However, its fluctuations decreased with Ro and, at $Ro < 0.02$, the blocked flow became time-independent and exhibited two-fold symmetry in space.

In a regime intermediate between that of

nearly zonal and blocked flows (Fig. 4), spontaneous transitions occurred between distinct zonal and blocked flows (Fig. 5A) for fixed experimental conditions (Ro and Ek). Similar spontaneous transitions appear in the atmosphere (4, 5), as well as in simple deterministic models with a sufficient number of degrees of freedom (12, 14, 16). Our blocked and zonal flows, however, both persisted for many more annulus rotation periods than did

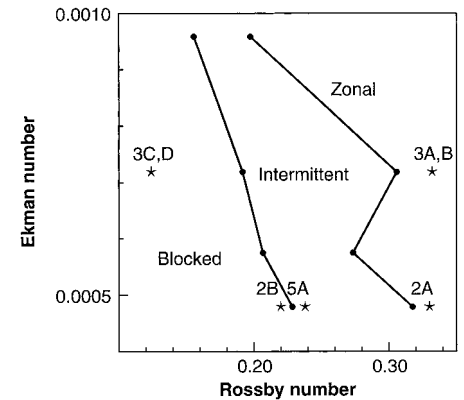


Fig. 4. Diagram showing boundaries between the three observed flow regimes: pure zonal, pure blocked, and intermittent regime. In the intermittent regime, spontaneous switching between blocked and zonal flows occurs at irregular intervals. Stars indicate the positions in this diagram of the experimental runs used for Fig. 2, A and B; Fig. 3, A through D; and Fig. 5A. Multiple stable equilibria were not observed.

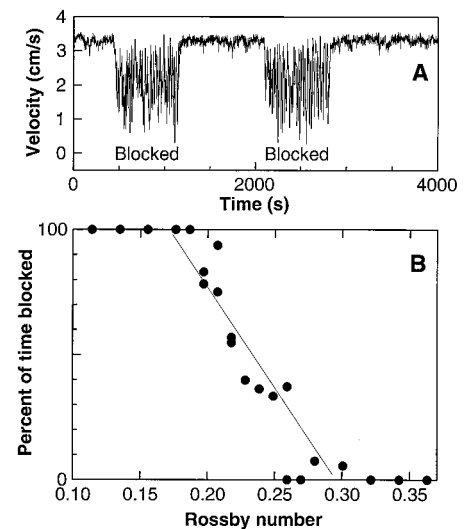
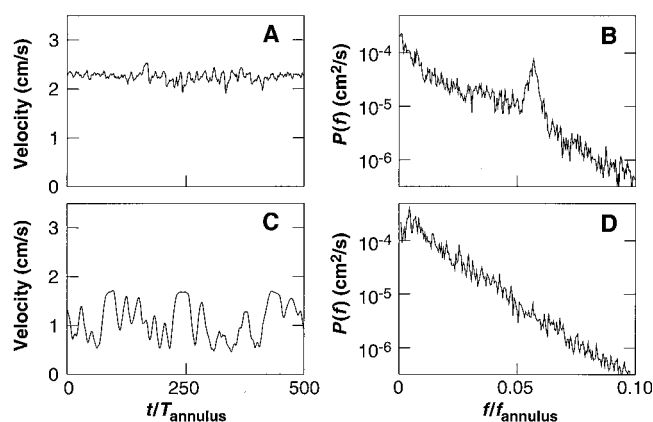


Fig. 5. (A) Velocity time series showing intermittent transitions between zonal and blocked flow (compare Figs. 3 and 4); $Ro = 0.237 \pm 0.005$ and $Ek = 4.8 \times 10^{-4}$ (pump flux $F = 280 \text{ cm}^3 \text{ s}^{-1}$ and $\Omega = 3\pi \text{ rad s}^{-1}$). (B) The fraction of time spent in the blocked state as a function of the Rossby number [compare with similar plots for the atmosphere (4) and barotropic models (12)]; $Ek = 7.2 \times 10^{-4}$ ($\Omega = 2\pi \text{ rad s}^{-1}$). To guide the eye, the straight line shows the least-squares fit to the intermittent data.

Fig. 3. (A and C) Velocity time series and (B and D) associated power spectra obtained from a hot-film probe located in the lid at $r = 2.5r_1$. Zonal (A and B) and blocked (C and D) flows correspond to $Ro = 0.332 \pm 0.005$ and 0.124 ± 0.005 , respectively (pump flux $F = 320$ and $120 \text{ cm}^3 \text{ s}^{-1}$, respectively), with $Ek = 7.2 \times 10^{-4}$ for both flows ($\Omega = 2\pi \text{ rad s}^{-1}$).



blocked and zonal flows in atmospheric observations. The absence of baroclinic instabilities in our annulus [compare with (18), for instance], and the greater stability of the experimental zonal flow (12) is presumably the cause of this discrepancy.

We conjecture that in the experiment, there are two basins of attraction, zonal and blocked (12, 15), connected by heteroclinic orbits. Similar switches between flow regimes—characterized there by distinct wavenumbers—have been observed in the thermally driven annulus, even in the absence of topography (28). Chaotic itinerancy (16, 29) provides a plausible scenario for such sporadic transitions; confirmation of such a scenario is left for further experiments and numerical simulations (30).

In the intermediate regime of Fig. 4, the fraction of time spent in one state varied as a function of the Rossby number (Fig. 5B). Similarly, as the pole-to-equator temperature gradient changes—from season to season or year to year in the same season (8, 12, 15, 16, 26, 27)—the relative prevalence of zonal- or blocked-flow episodes can change. Our results and idealized barotropic models (12) agree in that the frequency of blocking events increased when approaching the parameter range where blocking is the stable regime [see also (15)]. The seasonal and interannual variability of persistent nonzonal flow patterns, such as blocking, in the atmosphere is subtler and has been documented to some extent in the Pacific–North American sector, for both observations and general circulation models (31).

Our results provide new criteria by which topographic effects on low-frequency atmospheric, oceanic, and laboratory flows can be distinguished from thermal- and eddy-forcing effects.

REFERENCES AND NOTES

- J. G. Charney, *J. Meteorol.* **4**, 135 (1947); E. T. Eady *Tellus* **1**, 33 (1949).
- A. E. Gill, *Atmosphere-Ocean Dynamics* (Academic Press, San Diego, CA, 1982); J. R. Holton, *An Introduction to Dynamic Meteorology* (Academic Press, San Diego, CA, ed. 3, 1992); J. Pedlosky, *Geophysical Fluid Dynamics* (Springer-Verlag, New York, ed. 2, 1987).
- J. F. O'Connor, *Mon. Weather Rev.* **91**, 209 (1963).
- R. M. Dole and N. M. Gordon, *ibid.* **111**, 1567 (1983).
- X. Cheng and J. M. Wallace, *J. Atmos. Sci.* **50**, 2674 (1993); M. Kimoto and M. Ghil, *ibid.*, p. 2625.
- M. S. Tracton *et al.*, *Mon. Weather Rev.* **117**, 1604 (1989); F. Molteni and T. N. Palmer, *Q. J. R. Meteorol. Soc.* **119**, 269 (1993).
- R. Benzi, B. Saltzman, A. C. Wiin-Nielsen, Eds., *Anomalous Atmospheric Flows and Blocking*, vol. 29 of *Advances in Geophysics* (Academic Press, Orlando, FL, 1986).
- J. G. Charney and J. G. DeVore, *J. Atmos. Sci.* **36**, 1205 (1979).
- N.-C. Lau and M. J. Nath, *Mon. Weather Rev.* **115**, 251 (1987).
- J. Pedlosky, *J. Atmos. Sci.* **38**, 2626 (1981).
- R. Benzi, P. Malguzzi, A. Speranza, A. Sutera, *Q. J. R. Meteorol. Soc.* **112**, 661 (1986).
- B. Legras and M. Ghil, *J. Atmos. Sci.* **42**, 433 (1985).

- S. L. Marcus, M. Ghil, J. O. Dickey, *ibid.* **53**, 1993 (1996).
- B. B. Reinhold and R. P. Pierrehumbert, *Mon. Weather Rev.* **110**, 1105 (1982).
- T. N. Palmer, *Bull. Am. Meteorol. Soc.* **74**, 49 (1993).
- H. Itoh and M. Kimoto, *J. Atmos. Sci.* **53**, 2217 (1996).
- R. Hide, *Philos. Trans. R. Soc. London Ser. A* **250**, 442 (1958); E. N. Lorenz, *The Nature and Theory of the General Circulation of the Atmosphere* (World Meteorological Organization, Geneva, 1967).
- P. R. Jonas, *Q. J. R. Meteorol. Soc.* **107**, 775 (1981); G. Q. Li, R. Kung, R. L. Pfeffer, *J. Atmos. Sci.* **43**, 2585 (1986); P. Bernardet, A. Butet, M. Déqué, M. Ghil, R. L. Pfeffer, *ibid.* **47**, 3023 (1990); J. M. Pratte and J. E. Hart, *J. Fluid Mech.* **229**, 87 (1991).
- A previous barotropic simulation and experiment [G. F. Carnevale, R. C. Kloosterziel, G. J. F. van Heijst, *J. Fluid Mech.* **233**, 119 (1991)] examined local vortex motion over topography but did not address low-frequency variability of global flows.
- J. Sommeria, S. D. Meyers, H. L. Swinney, *Nature* **337**, 58 (1989).
- T. H. Solomon, W. J. Holloway, H. L. Swinney, *Phys. Fluids A* **5**, 1971 (1993).
- J. Sommeria, S. D. Meyers, H. L. Swinney, *Nonlinear Topics in Ocean Physics*, A. R. Osborne, Ed. (North-Holland, Amsterdam, 1991), pp. 227–269.
- M. S. Pervez and T. H. Solomon, *Exp. Fluids* **17**, 135 (1994).
- E. R. Weeks, thesis, University of Texas, Austin (1997).
- E. Kalnay-Rivas and L.-O. Merkin, *J. Atmos. Sci.* **38**, 2077 (1981).
- C.-G. Rossby *et al.*, *J. Mar. Res.* **2**, 38 (1939); D. F. Rex *Tellus* **2**, 275 (1950).
- C. M. Strong, F.-f. Jin, M. Ghil, *J. Atmos. Sci.* **52**, 2627 (1995).
- R. Hide and P. J. Mason, *Adv. Phys.* **24**, 47 (1975); W.-G. Früh and P. L. Read, *Philos. Trans. R. Soc. London Ser. A* **355**, 101 (1997).
- K. Kaneko, *Physica D* **41**, 137 (1990); *ibid.* **54**, 5 (1991).
- Y. Tian, thesis, University of California, Los Angeles (1997); Y. Tian *et al.*, in preparation.
- J. D. Horel and C. R. Mechoso, *J. Clim.* **1**, 582 (1988).
- J. M. Wallace and M. L. Blackmon, in *Large-Scale Dynamical Processes in the Atmosphere*, B. J. Hoskins and R. P. Pearce, Eds. (Academic Press, London, 1983), pp. 55–94; I. M. Held, *ibid.*, pp. 127–168.
- We thank C. Baroud, M. Kimoto, P. Klein, L. Panetta, P. L. Read, D. Tritton, and three anonymous referees for helpful comments. K. Hartman and G. Llamas helped with the text and W. Weibel with the figures. The experiments were supported by the Office of Naval Research (ONR). The University of California Los Angeles investigators were supported by NSF; M.G. was also supported by the Elf-Aquitaine/CNRS Chair of the Académie des Sciences, Paris. E.R.W. acknowledges the support of an ONR Augmentation Award for Science and Engineering Training and a University of Texas Livingston Fellowship.

22 July 1997; accepted 17 October 1997

Reversible Polymers Formed from Self-Complementary Monomers Using Quadruple Hydrogen Bonding

Rint P. Sijbesma, Felix H. Beijer, Luc Brunsveld, Brigitte J. B. Folmer, J. H. K. Ky Hirschberg, Ronald F. M. Lange, Jimmy K. L. Lowe, E. W. Meijer*

Units of 2-ureido-4-pyrimidone that dimerize strongly in a self-complementary array of four cooperative hydrogen bonds were used as the associating end group in reversible self-assembling polymer systems. The unidirectional design of the binding sites prevents uncontrolled multidirectional association or gelation. Linear polymers and reversible networks were formed from monomers with two and three binding sites, respectively. The thermal and environmental control over lifetime and bond strength makes many properties, such as viscosity, chain length, and composition, tunable in a way not accessible to traditional polymers. Hence, polymer networks with thermodynamically controlled architectures can be formed, for use in, for example, coatings and hot melts, where a reversible, strongly temperature-dependent rheology is highly advantageous.

Noncovalent interactions are increasingly being used in the molecular self-assembly of well-defined supramolecular structures and materials. Such interactions are important in polymer science, where hydrogen bonding and other weak reversible interactions are important in determining polymer prop-

erties and in the design of new polymer architectures (1, 2). However, the interactions used always rely on the cooperative phenomenon of many weak interactions, which lack directionality, giving rise to microphase-separated structures or gelation due to network formation (3). For linear supramolecular polymers (4), it is a prerequisite to have strong and highly directional, reversible interactions in order to construct materials that include a reversible alternative for the covalent bond. This concept has been known for years (5–13), but polymers with appreciable degrees of polymerization in the amorphous state or even in

R. P. Sijbesma, F. H. Beijer, L. Brunsveld, B. J. B. Folmer, J. H. K. Ky Hirschberg, J. K. L. Lowe, E. W. Meijer, Laboratory of Organic Chemistry, Eindhoven University of Technology, Post Office Box 513, 5600 MB Eindhoven, Netherlands.
R. F. M. Lange, DSM Research, Post Office Box 18, 6160 MD Geleen, Netherlands.

*To whom correspondence should be addressed. E-mail: tegtobm@chem.tue.nl